Optomechanically-induced-transparency cooling of massive mechanical resonators to the quantum ground state

LIU Yong-Chun[1], XIAO Yun-Feng[1*], LUAN Xingsheng[2] & WONG Chee Wei[2*]

[1]*State Key Laboratory for Mesoscopic Physics and School of Physics, Peking University; Collaborative Innovation Center of Quantum Matter, Beijing 100871, China;*
[2]*Optical Nanostructures Laboratory, Columbia University, New York, NY 10027, USA*

Ground state cooling of massive mechanical objects remains a difficult task restricted by the unresolved mechanical sidebands. We propose an optomechanically-induced-transparency cooling scheme to achieve ground state cooling of mechanical motion without the resolved sideband condition in a pure optomechanical system with two mechanical modes coupled to the same optical cavity mode. We show that ground state cooling is achievable for sideband resolution ω_m/κ as low as ~ 0.003. This provides a new route for quantum manipulation of massive macroscopic devices and high-precision measurements.

ground state cooling, resolved sideband limit, optomechanics

PACS number(s): 42.50.Wk, 07.10.Cm, 42.50.Lc

1 Introduction

Cavity optomechanics provides a perfect platform not only for the fundamental study of quantum theory but also for the broad applications in quantum information processing and high-precision metrology [1–3]. For most applications it is highly desirable to cool the mechanical motion to the quantum ground state by suppressing thermal noise. In the past few years numerous efforts have made strides towards this goal through backaction cooling [4–13]. However, the cooling limit is subjected to quantum backaction, and ground state cooling is possible only in the resolved sideband (good-cavity) limit [14,15], which requires the resonance frequency of the mechanical motion (ω_m) to be larger than the cavity decay rate κ. This sets a major obstacle for the ground state preparation and quantum manipulation of macroscopic and mesoscopic mechanical resonators with typically low mechanical resonance frequency. Therefore, it is essential to overcome this limitation, so that ground state cooling can be achieved irrespective of mechanical resonance frequency and cavity damping.

Some recent proposals [16] focus on circumventing the resolved sideband restriction by using dissipative coupling mechanism [17,18], parameter modulations [19–23] and hybrid systems [24–29]. Here we propose a unresolved-sideband ground-state cooling scheme in a generic optomechanical system which does not require modified mechanisms of coupling or specific modulation of the system parameters, or additional components. We take advantage of the destructive quantum interference in a cavity optomechanical system with two mechanical modes coupled to the same optical cavity mode, where optomechanically-induced transparency (OMIT) phenomenon [30–33] occurs. We show that with the help of quantum interference, ground state cooling of the mechanical mode with $\omega_m \ll \kappa$ can be achieved. Moreover, we

*Corresponding author (XIAO YunFeng, email: yfxiao@pku.edu.cn; WONG CheeWei, email: cww2014@columbia.edu)

examine the multiple input cascaded OMIT cooling which further suppresses the quantum backaction heating. This renders quantum optomechanics with low optical-Q cavities and low mechanical frequency resonators.

2 Model

In a generic optomechanical system, as shown in Figure 1(a), we consider an optical cavity mode a coupled to two mechanical resonance modes b and c, where b is the mode to be cooled and c is a control mode. The cavity is driven by a cooling laser and a control laser, with frequencies ω_0 and ω_1, respectively. In the frame rotating at the cavity resonance frequency ω_c, the system Hamiltonian reads as:

$$
\begin{aligned}
H &= H_b + H_c, \\
H_b &= \omega_m b^\dagger b + g a^\dagger a (b + b^\dagger) + (\Omega_0^* a e^{i\Delta_0 t} + \text{H.c.}), \\
H_c &= \omega_{mc} c^\dagger c + g_c a^\dagger a (c + c^\dagger) + (\Omega_1^* a e^{i\Delta_1 t} + \text{H.c.}).
\end{aligned} \quad (1)
$$

Here H_b (H_c) describes the Hamiltonian related with mode b (c); ω_m (ω_{mc}) is the resonance frequency of mode b (c); g and g_c denote the single-photon optomechanical coupling rates; Ω_0 (Ω_1) represents the driving strength and $\Delta_0 = \omega_0 - \omega_c$ ($\Delta_1 = \omega_1 - \omega_c$) is the frequency detuning between the cooling (control) laser and the cavity mode. For strong driving, the linearized system Hamiltonian is given by

$$
\begin{aligned}
H_L &= \omega_m b_1^\dagger b_1 + [G^{(t)} a_1^\dagger + G^{(t)*} a_1](b_1 + b_1^\dagger) \\
&\quad + \omega_c c_1^\dagger c_1 + [G_c^{(t)} a_1^\dagger + G_c^{(t)*} a_1](c_1 + c_1^\dagger).
\end{aligned} \quad (2)
$$

Here the operators a_1, b_1 and c_1 describe the quantum fluctuations around the corresponding classical mean fields after the linearization; $G^{(t)} = g(\alpha_0 e^{-i\Delta_0' t} + \alpha_1 e^{-i\Delta_1' t})$ and $G_c^{(t)} = g_c(\alpha_0 e^{-i\Delta_0' t} + \alpha_1 e^{-i\Delta_1' t})$ are the light-enhanced optomechanical coupling strengths, with modified detunings $\Delta_0' = \Delta_0 + \Delta_{om}$, $\Delta_1' = \Delta_1 + \Delta_{om}$ and $\Delta_{om} = 2(g^2/\omega_m + g_c^2/\omega_{mc})(|\alpha_0|^2 + |\alpha_1|^2)$; α_0 and α_1 are the intracavity field from the contribution of the cooling and control laser inputs; κ, γ ($\equiv \omega_m/Q_m$) and γ_c ($\equiv \omega_{mc}/Q_{mc}$) are the energy decay rates of the modes a, b and c.

3 Quantum noise spectrum

The optical force acting on mode b takes the form $F = -[G^{(t)*} a_1 + G^{(t)} a_1^\dagger]/x_{ZPF}$, where x_{ZPF} is the zero-point fluctuation. The quantum noise spectrum of the optical force $S_{FF}(\omega) \equiv \int dt e^{i\omega t} \langle F(t) F(0) \rangle$ is calculated to be

$$
\begin{aligned}
S_{FF}(\omega) &= \sum_{j=0}^1 S_{FF}^j(\omega), \\
S_{FF}^j(\omega) &= \frac{g^2}{x_{ZPF}^2} |\alpha_j \tilde{\chi}_j(\omega)|^2 \\
&\quad \times \left[\kappa + g_c^2 \sum_{k=0}^1 |\alpha_k|^2 \tilde{\chi}_{mc}(\omega + \Delta_j' - \Delta_k') \right],
\end{aligned} \quad (3)
$$

where $\tilde{\chi}_j^{-1}(\omega) = \chi_j^{-1}(\omega) + g_c^2 \sum_{k=0}^1 |\alpha_k|^2 [\chi_{mc}(\omega + \Delta_j' - \Delta_k') + \chi_{mc}^*(-\omega - \Delta_j' + \Delta_k')]$, $\tilde{\chi}_{mc}(\omega) = \gamma_c(n_{c,th} + 1)|\chi_{mc}(\omega)|^2 + \gamma_c n_{c,th}|\chi_{mc}(-\omega)|^2$, $\chi_j^{-1}(\omega) = -i(\omega + \Delta_j') + \kappa/2$ and $\chi_{mc}^{-1}(\omega) = -i(\omega - \omega_{mc}) + \gamma_c/2$, with integers j and k being the summation indices. Here $\chi_j(\omega)$ represent the optical response to the input light and $\chi_{mc}(\omega)$ is the response function of the control mechanical mode; $n_{th} = 1/[e^{\hbar\omega_m/(k_B T)} - 1]$ and $n_{c,th} = 1/[e^{\hbar\omega_{mc}/(k_B T)} - 1]$ are the thermal phonon numbers of modes b and c at the environmental temperature T.

In conventional single mechanical mode approach, the quantum noise spectrum exhibits a standard Lorentzian curve [15]. However, here due to the interaction between the control mechanical and the optical cavity modes, the noise spectrum (eq. (3)) is modified to a non-Lorentzian lineshape. This originates from the quantum interference manifested by OMIT. As shown in Figure 1(b), the system here contains a series of three-level subsystems relevant with OMIT for heating suppression. In the presence of the control field, the transition amplitude between the two pathways (red dashed arrow and blue dotted arrow) destructively interfere, leading to the suppression of the heating transition.

For the unresolved sideband regime ($\omega_m \ll \kappa$), the quantum noise spectra are plotted in Figure 2 with parameters $\omega_m/$
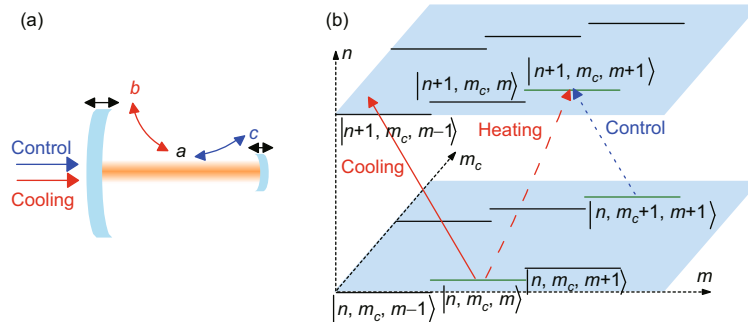
Figure 1 (a) Sketch of a typical optomechanical system with two mechanical modes b and c coupled to the same optical cavity mode a. The cavity is driven by a cooling laser and a control laser. (b) Energy level diagram of the system. $|n, m_c, m\rangle$ denotes the state of n photons, m_c c-mode phonons and m b-mode phonons in the displaced frame. The red solid (dashed) arrow denotes the cooling (heating) process of mode b. The blue dotted arrow denotes the control laser enhanced coupling between mechanical mode c and the optical cavity mode a.
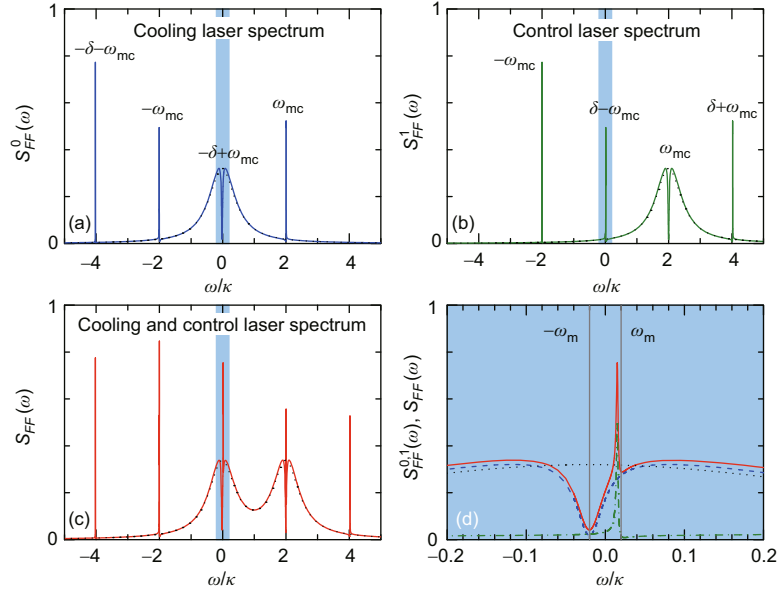
Figure 2   Quantum noise spectra (arbitrary units). The solid curves denote (a) $S_{FF}^0(\omega)$, (b) $S_{FF}^1(\omega)$ and (c) $S_{FF}(\omega)$ for $\omega_m/\kappa = 0.02$, $\omega_{mc}/\kappa = 2$, $\Delta_0' = \omega_m$, $\Delta_1' = -\omega_{mc}$, $g/\omega_m = 10^{-3}$, $g_c/\omega_{mc} = 5 \times 10^{-4}$, $\alpha_0 = \alpha_1 = 10^3$, $Q_{mc} = 10^4$ and $n_{th} = 10^3$. The black dotted curves in (a)–(c) correspond to the results without the control mode ($g_c = 0$). In (a) and (b), the position of the sharp peaks and dips are marked. (d) Zoom-in view of the shaded region in (a)–(c). $S_{FF}^0(\omega)$, blue dashed curve; $S_{FF}^1(\omega)$, green dashed-dotted curve; $S_{FF}(\omega)$, red solid curve. The black dotted curves corresponds to the result without the control mode and the control laser [$S_{FF}^{0,0}(\omega)$]. The gray vertical lines denote $\omega = \pm\omega_m$.

$\kappa = 0.02$, $\omega_{mc}/\kappa = 2$, $\Delta_0' = \omega_m$, $\Delta_1' = -\omega_{mc}$, $g/\omega_m = 10^{-3}$, $g_c/\omega_{mc} = 5 \times 10^{-4}$, $\alpha_0 = \alpha_1 = 10^3$, $Q_{mc} = 10^4$ and $n_{th} = 10^3$. Note that $S_{FF}^0(\omega)$ corresponds to the spectrum associated with the cooling laser (with detuning Δ_0') and $S_{FF}^1(\omega)$ represents the spectrum related to the control laser (with detuning Δ_1'). Without the control mechanical mode ($g_c = 0$), they reduce to $S_{FF}^{0,0}(\omega) = \kappa |\alpha_0\chi_0(\omega)|^2 g^2/x_{ZPF}^2$ and $S_{FF}^{1,0}(\omega) = \kappa |\alpha_1\chi_1(\omega)|^2 g^2/x_{ZPF}^2$, which are Lorentzians with the centers at $\omega = -\Delta_0'$ and $-\Delta_1'$ (black dotted curves in Figures 2(a) and (b)), respectively. In contrast, with the presence of the control mode, a series of OMIT resonances appear in the spectra. For $S_{FF}^0(\omega)$, those dips/peaks are located at $\omega = \pm \omega_{mc}$, $-\delta \pm \omega_{mc}$ (Figure 2(a)), where $\delta \equiv \Delta_0' - \Delta_1'$ represents the two-photon detuning of the input lasers. Thereinto, the resonances at $\omega = \pm \omega_{mc}$ originate from the interaction between the cooling laser and mode c, which changes the mode density for the cavity field to absorb/emit a phonon with energy $\hbar\omega_{mc}$; the resonances at $\omega = -\delta \pm \omega_{mc}$ stem from the interaction among the cooling laser, the control laser and mode c. Analogously, for $S_{FF}^1(\omega)$, the resonances are located at $\omega = \pm \omega_{mc}$, $\delta \pm \omega_{mc}$ (Figure 2(b)). For cooling of mode b, the dips/peaks at $\omega = \pm\omega_m$ are relevant, since $A_{\mp} \equiv S_{FF}(\pm\omega_m) x_{ZPF}^2$ are the rates for absorbing and emitting a b-mode phonon by the cavity field, corresponding to the cooling and heating of mode b, respectively. With the appropriate value of the two-photon detuning at $\delta = \omega_{mc} + \omega_m$, the OMIT lineshapes in $S_{FF}(\omega)$ can be tuned to appear at $\omega = \pm\omega_m$, as shown in Figures 2(c) and (d). At $\omega = -\omega_m$, it exhibits a deep OMIT window, which reveals the suppression of heating process, originating from the destructive interference. Although a shallow dip also appears

at $\omega = \omega_m$, it only slightly decreases the mode density. The reason is that, with $|\Delta_1'| \gg |\Delta_0'|$, this dip is located far away from the center ($\omega = -\Delta_1'$) of the Lorentzian background in $S_{FF}^{1,0}(\omega)$, as shown in Figure 2(b).

4   Covariance approach

To verify the destructive quantum interference effect, we next solve the quantum master equation and use covariance approach [34,35] to obtain exact numerical results. The master equation is given by $\dot\rho = i[\rho, H_L] + \kappa\mathcal{D}[a_1]\rho + \gamma(n_{th} + 1)\mathcal{D}[b_1]\rho + \gamma n_{th}\mathcal{D}[b_1^\dagger]\rho + \gamma_c(n_{c,th} + 1)\mathcal{D}[c_1]\rho + \gamma_c n_{c,th}\mathcal{D}[c_1^\dagger]\rho$, where $\mathcal{D}[\hat{o}]\rho = \hat{o}\rho\hat{o}^\dagger - (\hat{o}^\dagger\hat{o}\rho + \rho\hat{o}^\dagger\hat{o})/2$ denotes the the standard dissipator in Lindblad form. In Figures 3(a) and (b) we plot the time evolution of the mean phonon number $n_b(t)$ for typical parameters. For single mechanical mode case in the unresolved sideband regime, with red detuning input laser, the mechanical motion is only slowly cooled with a small cooling rate (net optical damping rate) $\Gamma_{opt} \equiv A_- - A_+$, without reaching the ground state. However, in the presence of the control mode and the control laser, the cooling rate can be enhanced for more than two orders of magnitude (Figure 3(c)), and ground state cooling with mean phonon number $n_b < 1$ is achievable, even for sideband resolution ω_m/κ as small as 0.02. It should be emphasized that in this case the cooling laser is blue detuned, which is quite different from the single mechanical mode approach. For the latter, blue detuning leads to amplification instead of cooling of the mechanical motion. The blue-detuning cooling is the unique property originating from the quantum interference which modifies the
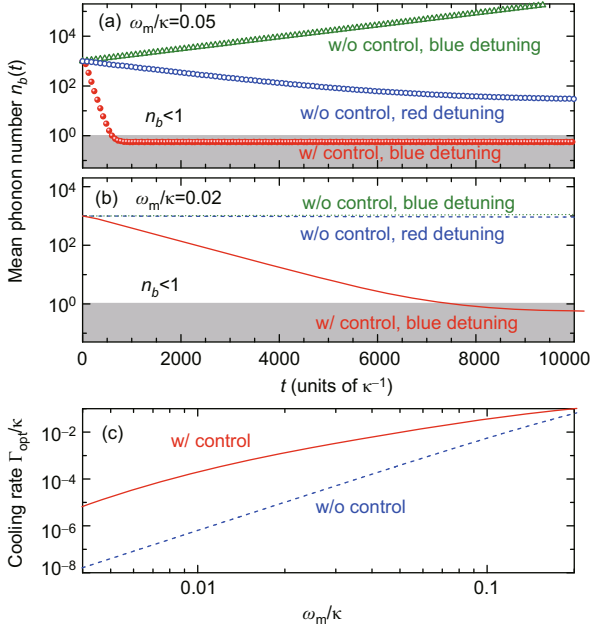
Figure 3 (a) Time evolution of the mean phonon number $n_b(t)$ with control mode (red closed circle) for $\omega_m/\kappa = 0.05$, $\omega_{mc}/\kappa = 2$, $\Delta'_0 = \omega_m$, $\Delta'_1 = -\omega_{mc}$, $g/\omega_m = 10^{-3}$, $g_c/\omega_{mc} = 5 \times 10^{-4}$, $\alpha_0 = 1200$, $\alpha_1 = 1600$, $Q_{mc} = 10^4$, $Q_m = 10^5$ and $n_{th} = 10^3$. The results without the control mode and the control laser ($g_c = 0$, $\alpha_1 = 0$) for $\Delta'_0 = -\omega_m$ (blue open circle) and $\Delta'_0 = \omega_m$ (green triangles) are plotted for comparison. (b) Same as (a) except that $\omega_m/\kappa = 0.02$ and $\alpha_0 = \alpha_1 = 10^3$. The shaded regions in (a) and (b) denote $n_b < 1$. (c) Cooling rates Γ_{opt} as functions of ω_m in the unit of κ with the presence (red solid curve) and absence (blue dashed curve) of the control mode and the control laser; the parameters are the same as Figure 3(b).

noise spectrum of the optical force. The OMIT lineshape can be viewed as the inverse of the standard Lorentzian, thus the detunings for cooling are just opposite to that for the single mechanical mode case.

5 Cascaded OMIT cooling

To further suppress quantum backaction heating, we propose the use of additional coherent laser inputs, resulting in cascaded OMIT cooling. For N inputs, the quantum noise spectrum of the optical force takes the same form as eq. (3) except that the summation indices (j, k) run from 0 to $N - 1$. As displayed in Figures 4(a)–(d), for two inputs, the suppression of heating for mode b is the contribution of suppressed $A^0_+ \equiv S^0_{FF}(-\omega_m) x^2_{ZPF}$, while $A^1_- \equiv S^1_{FF}(\omega_m) x^2_{ZPF}$ is also slightly suppressed. In the presence of the third input laser with detuning $\Delta'_2 = \Delta'_0 - 2(\omega_{mc} + \omega_m)$, the interaction involved with the control mode results in the suppression of $A^1_+ \equiv S^1_{FF}(-\omega_m) x^2_{ZPF}$ and $A^2_- \equiv S^2_{FF}(\omega_m) x^2_{ZPF}$. This results in the net optical damping rate $\Gamma_{opt} \equiv \sum^2_{k=0}(A^k_- - A^k_+) \simeq A^0_- - A^2_+$ (Figures 4(c) and (d)). More generally, for N inputs with detuning $\Delta'_k = \Delta'_0 - k(\omega_{mc} + \omega_m)$ ($k = 1, 2, \ldots, N-1$), we obtain $\Gamma_{opt} \simeq A^0_- - A^{N-1}_+$. Note that the remaining heating rate A^{N-1}_+ is much smaller than the original heating rate due to the large detuning Δ'_k for the $(N - 1)$-th input. In Figure 4(e) we com-
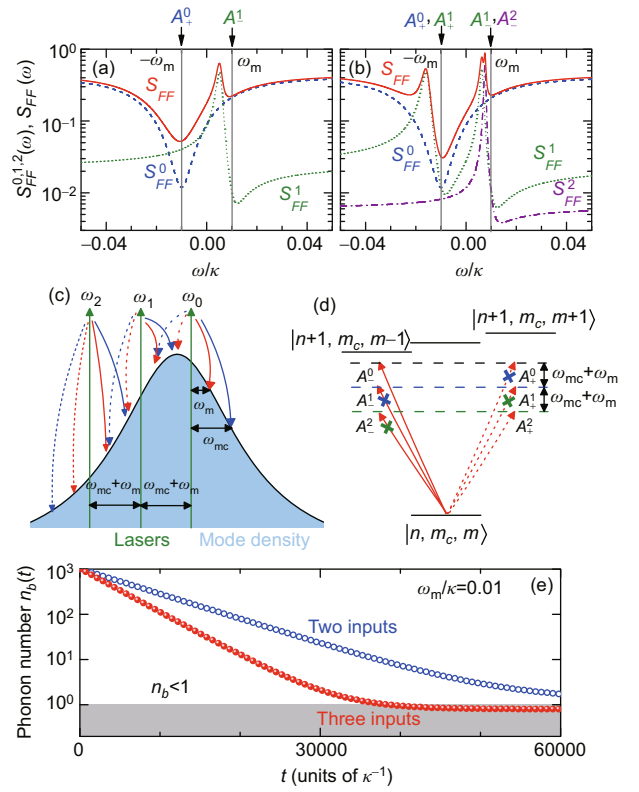

Figure 4 (a) and (b): Quantum noise spectra (arbitrary units) for two inputs (a) and three inputs (b). $S_{FF}(\omega)$, red solid curve; $S^0_{FF}(\omega)$, blue dashed curve; $S^1_{FF}(\omega)$, green dotted curve; $S^2_{FF}(\omega)$, purple dashed-dotted curve. The gray vertical lines denote $\omega = \pm\omega_m$. (c) Scattering interpretation of optomechanical interactions with three inputs. The shaded Lorentzian represents the mode density of the optical cavity. The green vertical arrows denote the input lasers. The solid (dashed) curved arrows denote the anti-Stokes (Stokes) scattering processes relevant with mode b (red) and mode c (blue). (d) Energy levels and interpretation of the suppression (denoted by the "×") of heating and cooling with three inputs. (e) Time evolution of the mean phonon number $n_b(t)$ with two inputs (blue open circle) and three inputs (red closed circle). The shaded region denotes $n_b < 1$. Here $\alpha_2 = 10^3$, $\omega_{mc}/\kappa = 2$, $\omega_m/\kappa = 0.01$ and other parameters are the same as Figure 3(b).

pare the cooling dynamics between two inputs and three inputs for typical parameters, which shows that the cascaded OMIT cooling enables larger cooling rate and lower cooling limit, with ground state cooling achievable even for $\omega_m/\kappa = 0.01$.

6 Cooling limits

In Figure 5 the fundamental cooling limits n_{min} as functions of the sideband resolution ω_m/κ are plotted. The exact numerical results are obtained from master equation simulations. The black dotted curve shows the best result for conventional single mechanical mode approach, given by $n_{min} = \kappa/(4\omega_m)$, which is obtained when $\Delta'_0 = -\kappa/2$ [14]. It reveals the great advantage of OMIT cooling and cascaded OMIT cooling, with possibility for ground state cooling even when $\omega_m/\kappa \sim 3 \times 10^{-3}$, which goes beyond the resolved sideband limit by nearly 3 orders of magnitude. Note that Figure 5
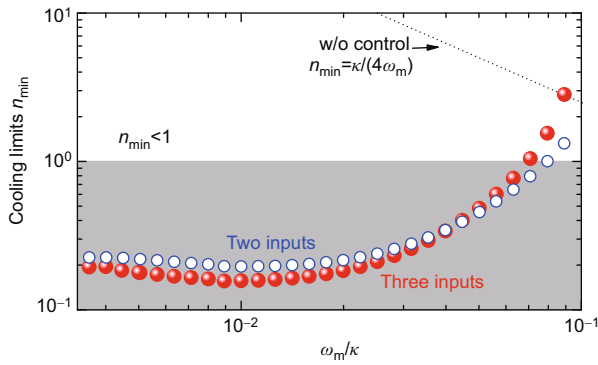
Figure 5   Fundamental cooling limits $n_{\min}$ as functions of $\omega_{\mathrm{m}}/\kappa$ for two inputs (red closed circles) and three inputs (blue open circles). The result for single mechanical mode approach (black dotted curve) is plotted for comparison. The shaded region denotes $n_{\min} < 1$. Here $\alpha_0 = \alpha_1 = \alpha_2 = 500$ and other parameters are the same as Figure 4.

shows the cooling limits increase as $\omega_{\mathrm{m}}/\kappa$ increases from ~ 0.02 to a larger value. This is a result of blue detuning induced heating, which becomes significant when $\omega_{\mathrm{m}}/\kappa$ is large.

7   Experimental feasibility

It should be stressed that the OMIT cooling described here adds little complexity to the existing optomechanical system, which is crucial in the experimental point of view. Compared with the conventional backaction cooling approach, the additional requirement here is a control mechanical mode and one (or more) input laser. It is experimentally feasible for various optomechanical systems within current technical conditions. On one hand, many optomechanical systems possess abundant mechanical modes with different resonance frequencies, since the oscillation have different types and orders. This situation can be found in optomechanical systems using whispering-gallery microcavities [36,37], photonic crystal cavities [38,39], membranes [40,41], nanostrings [42] and nanorods [43,44] amongst others. Usually only one mechanical mode is used in most optomechanical experiments, while exciting an additional mechanical mode is often unintended. On the other hand, composite optomechanical systems, containing two independent mechanical resonators, are also conceivable. For example, in Fabry-Pérot cavities, the motion of one mirror acts as an control mechanical mode while the other mirror is to be cooled (Figure 1(a)). In the near-field optomechanical system [42], to cool the nanostrings, the control mode can be selected from the vibration of the microtoroid.

8   Conclusion

In summary, we have presented the OMIT cooling scheme allowing ground state cooling of mechanical resonators beyond the resolved sideband limit. It is demonstrated that by employing the OMIT interference, quantum backaction heating can be largely suppressed, extending the fundamental limit

of backaction cooling. The scheme is experimentally feasible, which requires another control mechanical mode and multiple laser inputs. Such a M-O-M system (M, mechanical mode; O, optical mode) studied here offers potential for cooling enormous mass scale resonators [45,46], which possess small resonance frequencies. Together with the recently examined multi-optical-mode [28,47–50] and multi-mechanical-mode [51–55] systems,it is shown that such interference effect in multi-mode cavity optomechanics provides unique advantage for both fundamental studies and broad applications. Recently we noticed a related work [56], but here we use the covariance approach to examine the fundamental cooling limits and present detailed analysis of cascaded OMIT cooling. This paves the way for the manipulation of macroscopic mechanical resonators in the quantum regime.

1   Kippenberg T J, Vahala K J. Cavity optomechanics: Back-action at the mesoscale. Science, 2008, 321: 1172–1176

2   Aspelmeyer M, Kippenberg T J, Marquardt F. Cavity optomechanics. arXiv:1303.0733

3   Meystre P. A short walk through quantum optomechanics. Ann Phys, 2013, 525: 215–233

4   Teufel J D, Donner T, Li D, et al. Sideband cooling of micromechanical motion to the quantum ground state. Nature, 2011, 475: 359–363

5   Chan J, Mayer A T P, Safavi-Naeini A H, et al. Laser cooling of a nanomechanical oscillator into its quantum ground state. Nature, 2011, 478: 89–92

6   Gigan S, Böhm H R, Paternostro M, et al. Self-cooling of a micromirror by radiation pressure. Nature, 2006, 444: 67–70

7   Arcizet O, Cohadon P F, Briant T, et al. Radiation-pressure cooling and optomechanical instability of a micromirror. Nature, 2006, 444: 71–74

8   Schliesser A, Del'Haye P, Nooshi N, et al. Radiation pressure cooling of a micromechanical oscillator using dynamical backaction. Phys Rev Lett, 2006, 97: 243905

9   Schliesser A, Rivière R, Anetsberger G, et al. Resolved-sideband cooling of a micromechanical oscillator. Nat Phys, 2008, 4: 415–419

10   Gröblacher S, Hertzberg J B, Vanner M R, et al. Demonstration of an ultracold micro-optomechanical oscillator in a cryogenic cavity. Nat Phys, 2009, 5: 485–488

11   Park Y S, Wang H. Resolved-sideband and cryogenic cooling of an optomechanical resonator. Nat Phys, 2009, 5: 489–493

12   Schliesser A, Arcizet O, Rivère R, et al. Resolved-sideband cooling and position measurement of a micromechanical oscillator close to the Heisenberg uncertainty limit. Nat Phys, 2009, 5: 509–514

13   Rocheleau T, Ndukum T, Macklin C, et al. Preparation and detection of a mechanical resonator near the ground state of motion. Nature, 2010, 463: 72–75

14   Wilson-Rae I, Nooshi N, Zwerger W, et al. Theory of ground state cooling of a mechanical oscillator using dynamical backaction. Phys Rev Lett, 2007, 99: 093901

15 Marquardt F, Chen J P, Clerk A A, et al. Quantum theory of cavity-assisted sideband cooling of mechanical motion. Phys Rev Lett, 2007, 99: 093902

16 Liu Y C, Hu Y W, Wong C W, et al. Review of cavity optomechanical cooling. Chin Phys B, 2013, 22: 114213

17 Elste F, Girvin S M, Clerk A A. Quantum noise interference and back-action cooling in cavity nanomechanics. Phys Rev Lett, 2009, 102: 207209

18 Xuereb A, Schnabel R, Hammerer K. Dissipative optomechanics in a Michelson-Sagnac interferometer. Phys Rev Lett, 2011, 107: 213604

19 Tian L. Ground state cooling of a nanomechanical resonator via parametric linear coupling. Phys Rev B, 2009, 79: 193407

20 Li Y, Wu L A, Wang Z D. Fast ground-state cooling of mechanical resonators with time-dependent optical cavities. Phys Rev A, 2011, 83: 043804

21 Liao J Q, Law C K. Cooling of a mirror in cavity optomechanics with a chirped pulse. Phys Rev A, 2011, 84: 053838

22 Wang X, Vinjanampathy S, Strauch F W, et al. Ultraefficient cooling of resonators: Beating sideband cooling with quantum control. Phys Rev Lett, 2011, 107: 177204

23 Machnes S, Cerrillo J, Aspelmeyer M, et al. Pulsed laser cooling for cavity optomechanical resonators. Phys Rev Lett, 2012, 108: 153601

24 Genes C, Ritsch H, Vitali D. Micromechanical oscillator ground-state cooling via resonant intracavity optical gain or absorption. Phys Rev A, 2009, 80: 061803(R)

25 Vogell B, Stannigel K, Zoller P, et al. Cavity-enhanced long-distance coupling of an atomic ensemble to a micromechanical membrane. Phys Rev A, 2013, 87: 023816

26 Restrepo J, Ciuti C, Favero I. Single-polariton optomechanics. Phys Rev Lett, 2014, 112: 013601

27 Gu W J, Li G X. Quantum interference effects on ground-state optomechanical cooling. Phys Rev A, 2013, 87: 025804

28 Liu Y C, Xiao Y F, Luan X, et al. Ground state cooling of mechanical motion through coupled cavity interactions in the unresolved sideband regime. CLEO, 2013 (Optical Society of America). p.QM2B.2

29 Liu Y C, Xiao Y F, Luan X, et al. Coupled cavities for motional ground state cooling and strong optomechanical coupling. Phys Rev X, under review

30 Weis S, Rivière R, Deléglise S, et al. Optomechanically induced transparency. Science, 2010, 330: 1520–1523

31 Safavi-Naeini A H, Alegre T P M, Chan J, et al. Electromagnetically induced transparency and slow light with optomechanics. Nature, 2011, 472: 69–73

32 Agarwal G S, Huang S. Electromagnetically induced transparency in mechanical effects of light. Phys Rev A, 2010, 81: 041803(R)

33 Qu K, Agarwal G S. Phonon-mediated electromagnetically induced absorption in hybrid opto-electromechanical systems. Phys Rev A, 2013, 87: 031802(R)

34 Liu Y C, Xiao Y F, Luan X, et al. Dynamic dissipative cooling of a mechanical resonator in strong coupling optomechanics. Phys Rev Lett, 2013, 110: 153606

35 Liu Y C, Shen Y F, Gong Q, et al. Optimal limits of cavity optomechanical cooling in the strong coupling regime. Phys Rev A, 2014, 89: 053821

36 Kippenberg T J, Rokhsari H, Carmon T, et al. Analysis of radiation-pressure induced mechanical oscillation of an optical microcavity. Phys Rev Lett, 2005, 95: 033901

37 Tomes M, Carmon T. Photonic micro-electromechanical systems vibrating at X-band (11-GHz) rates. Phys Rev Lett, 2009, 102: 113601

38 Eichenfield M, Chan J, Camacho R M, et al. Optomechanical crystals. Nature, 2009, 462: 78–82

39 Zheng J, Li Y, Aras M S, et al. Parametric optomechanical oscillations in two-dimensional slot-type high-Q photonic crystal cavities. App Phys Lett, 2012, 100: 211908

40 Thompson J D, Zwickl B M, Jayich A M, et al. Strong dispersive coupling of a high-finesse cavity to a micromechanical membrane. Nature, 2008, 452: 72

41 Bui C H, Zheng J, Hoch S W, et al. High-reflectivity, high-Q micromechanical membranes via guided resonances for enhanced optomechanical coupling. App Phys Lett, 2012, 100: 021110

42 Anetsberger G, Arcizet O, Unterreithmeier Q P, et al. Near-field cavity optomechanics with nanomechanical oscillators. Nat Phys, 2009, 5: 909–914

43 Zheng J, Sun X, Li Y, et al. Femtogram dispersive L3-nanobeam optomechanical cavities: Design and experimental comparison. Opt Express, 2012, 20: 26484–26498

44 Li M, Pernice W H P, Xiong C, et al. Harnessing optical forces in integrated photonic circuits. Nature, 2008, 456: 480

45 Abbott B, Abbott R, Adhikari R, et al. Observation of a kilogram-scale oscillator near its quantum ground state. New J Phys, 2009, 11: 073032

46 Abbott B, Abbott R, Adhikari R, et al. LIGO: The laser interferometer gravitational-wave observatory. Rep Prog Phys, 2009, 72: 076901

47 Hill J T, Safavi-Naeini A H, Chan J, et al. Coherent optical wavelength conversion via cavity-optomechanics. Nat Commun, 2012, 3: 1196

48 Dong C, Fiore V, Kuzyk M C, et al. Optomechanical dark mode. Science, 2012, 338: 1609–1613

49 Liu Y, Davanco M, Aksyuk V, et al. Electromagnetically induced transparency and wideband wavelength conversion in silicon nitride microdisk optomechanical resonators. Phys Rev Lett, 2013, 110: 223603

50 Bagci T, Simonsen A, Schmid S, et al. Optical detection of radio waves through a nanomechanical transducer. Nature, 2014, 507: 81–85

51 Lin Q, Rosenberg J, Chang D, et al. Coherent mixing of mechanical excitations in nano-optomechanical structures. Nat Photon, 2010, 4: 236–242

52 Massel F, Cho S U, Pirkkalainen J M, et al. Multimode circuit optomechanics near the quantum limit. Nat Commun, 2012, 3: 987

53 Seok H, Buchmann L F, Singh S, et al. Optically mediated nonlinear quantum optomechanics. Phys Rev A, 2012, 86: 063829

54 Seok H, Buchmann L F, Wright E M, et al. Multimode strong-coupling quantum optomechanics. Phys Rev A, 2013, 88: 063809

55 Tan H, Li G, Meystre P. Dissipation-driven two-mode mechanical squeezed states in optomechanical systems. Phys Rev A, 2013, 87: 033829

56 Ojanen T, Børkje K. Ground-state cooling of mechanical motion in the unresolved sideband regime by use of optomechanically induced transparency. Phys Rev A, 2014, 90: 013824